JACS
JOURNAL OF THE AMERICAN CHEMICAL SOCIETY

COMMUNICATION

pubs.acs.org/JACS

Hydrogen Confinement in Carbon Nanopores: Extreme Densification at Ambient Temperature

Nidia C. Gallego,*[,†] Lilin He,[‡] Dipendu Saha,[†] Cristian I. Contescu,[†] and Yuri B. Melnichenko*[,‡]

[†]Materials Science and Technology Division and [‡]Neutron Scattering Sciences Division, Oak Ridge National Laboratory, Oak Ridge, Tennessee 37831, United States

Supporting Information

ABSTRACT: In-situ small-angle neutron scattering studies of H_2 confined in small pores of polyfurfuryl alcohol-derived activated carbon at room temperature have provided for the first time its phase behavior in equilibrium with external H_2 at pressures up to 200 bar. The data were used to evaluate the density of the adsorbed fluid, which appears to be a function of both pore size and pressure and is comparable to the density of liquid H_2 in narrow nanopores at ~200 bar. The surface−molecule interactions responsible for densification of H_2 within the pores create internal pressures that exceed the external gas pressure by a factor of up to ~50, confirming the benefits of adsorptive storage over compressive storage. These results can be used to guide the development of new carbon adsorbents tailored for maximum H_2 storage capacities at near-ambient temperatures.

A critical need in the development of new hydrogen storage media is detailed data on the density of adsorbed H_2 as a function of pore size, pressure, and temperature; however, such measurements have been an experimental challenge. This paper details the use of small-angle neutron scattering (SANS) to provide the first-ever experimental measurements of the phase behavior of H_2 confined in the pores of a carbon adsorbent as a function of pore size and pressure. The results provide evidence that adsorptive gas storage is more efficient at lower pressures and in pores with subnanometer width. The findings suggest a pathway for the synthesis of hydrogen storage materials that exceed U.S. Department of Energy (DOE) targets.

Entrapping H_2 within the nanopores of solid adsorbents by physisorption serves as an alternative option for on-board hydrogen storage for transportation applications.[1−6] The key advantage of the physisorption process for hydrogen storage is the much higher density of the adsorbed gas, which translates into higher storage capacities at lower pressures. The densification of H_2 (or any adsorbed gas in general) is due to the attractive forces between the gas molecules and the pore walls. As a consequence of these interactions, the pressure experienced by the gas molecules confined within the pores can be many times higher than the external gas pressure (P_{ext}). Tanaka et al.[7] presented indirect experimental evidence that H_2 confined in single-walled carbon nanohorns at 20 K is more densely packed than bulk liquid H_2, with a density approaching that of solid H_2. In a neutron diffraction study at 77 K, Liu et al.[8] reported that unsaturated metal sites in a metal−organic framework enhance the *surface* packing density of H_2 to values higher than that of solid H_2 at 4 K. Using quantum-chemical calculations and accounting for quantum effects at moderate temperatures, Patchkovskii et al.[9] predicted that H_2 molecules trapped between graphene layers can experience effective internal pressures (P_{int}) much higher than P_{ext} (up to ~55 times higher at P_{ext} = 5 MPa). They also calculated that the pressurization ratio P_{int}/P_{ext} increases with decreasing temperature and that it is highly dependent on the pore size. These results indicate that the graphene structure acts as a "nanopump" that densifies the confined gas. According to Peng and Morris,[10] P_{int} and P_{ext} are related by

$$P_{int} = P_{ext} \exp\left(-\frac{\Delta H}{RT}\right) \quad (1)$$

where $\Delta H < 0$ is the enthalpy of adsorption, R is the gas constant, and T is the temperature. Equation 1 is equivalent to setting the chemical potentials of the external and adsorbed gases equal and using pressure as an approximation for fugacity. Thus, at room temperature, $|\Delta H|$ must be ~7.5 kJ/mol to increase P_{int} by an order of magnitude (15 kJ/mol for 2 orders of magnitude). Since the adsorption potential in nanopores, and thus the densification factor, depends strongly on the width of the pores and the pressure, knowledge of the structural characteristics of the materials is crucial in selecting and/or designing the adsorbents for efficient hydrogen storage. First-principles calculations and Monte Carlo simulations have suggested that narrow micropores with subnanometer pore widths (6−7 Å; herein called nanopores) are the most effective for entrapping H_2 molecules.[11−13] Adsorption measurements[14,15] have confirmed that carbons with median pore widths of 6−7 Å exhibited the highest H_2 adsorption capacity; an average density for the adsorbed H_2 was calculated[15] by assuming that all molecules dwelled within the pores of a particular median width. However, assuming a single density value for adsorbed H_2 is an oversimplification that does not describe the local density in pores of varying sizes in a carbon with a wide pore size distribution.

Detailed information on the adsorbed phase density within pores of various sizes is a critical prerequisite for designing and developing the next generation of hydrogen storage materials; controlling the size and number of pores may lead to improved storage capacity and heat of adsorption. However, acquiring quantitative data on the density of adsorbed H_2 has

Received: March 17, 2011
Published: August 05, 2011

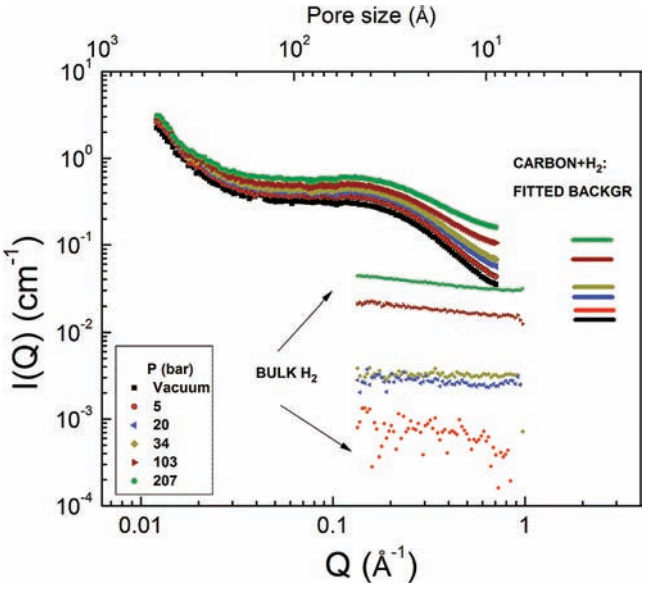

Figure 1. SANS patterns from PFAC under vacuum and at elevated pressures of H_2 at room temperature (raw data before correction for incoherent background). Scattering from bulk H_2 measured at the same pressures as the confined H_2 is also shown. Fitted values of the incoherent background at each pressure are shown at the right. The observed significant differences between the scattering from bulk H_2 and H_2-loaded carbon are due to the extreme hydrogen densification in small pores. All curves are color-coded.

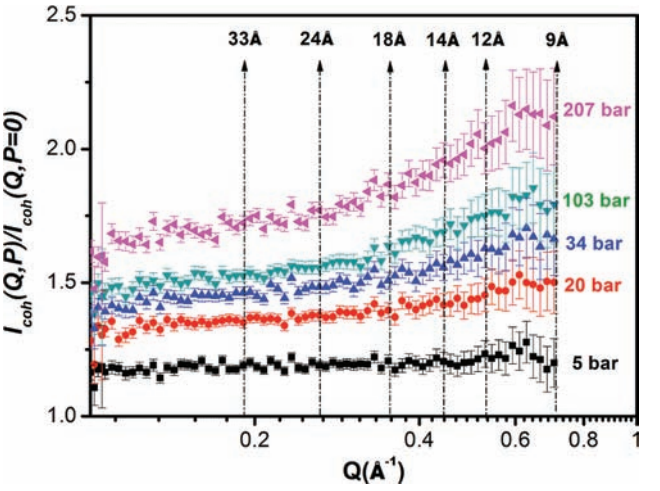

Figure 2. Ratios of coherent intensities measured for H_2-loaded and blank (under vacuum) carbon, $I_{coh}(Q, P)/I_{coh}(Q, P = 0)$. The Q values (and corresponding pore sizes) selected for density calculations are also shown.

remained an outstanding challenge because of numerous experimental complications. Recent studies have demonstrated that SANS can provide unique pore-size-specific information on the phase behavior of confined fluids and may be used to evaluate the density of the adsorbed fluid in pores of various sizes, including subnanometer length scales. To date this new methodology has been used to investigate the adsorption of supercritical CO_2 in engineered and natural porous materials such as silica aerogels and coal.[16−18] In this work, we extended the methodology to evaluate for the first time the density of adsorbed H_2 gas in the nanopores and mesopores of polyfurfuryl alcohol-derived activated carbon (PFAC). Furthermore, using an equation of state for H_2, we calculated the corresponding internal pressures experienced by the confined fluid.

The PFAC material was synthesized following a variation of the procedure of Burket et al.[19] and had a surface area of 1530 m^2/g and a pore volume of 0.68 cm^3/g, of which 90% was contained in micropores with widths of <20 Å. Synthesis and characterization details may be found in the Supporting Information (SI).

In-situ high-pressure SANS studies were conducted using the general-purpose SANS instrument at Oak Ridge National Laboratory (ORNL),[20] with a neutron wavelength (λ) of 4.8 Å ($\Delta\lambda/\lambda \approx 0.13$). The sample−detector distance was chosen to cover an overall range of scattering vectors (Q) of 0.01 Å^{-1} < Q < 0.8 Å^{-1}, where $Q = (4\pi/\lambda)\sin(\theta/2)$, in which θ is the scattering angle. The upper limit of Q, Q_{max}= 0.8 Å^{-1}, was determined by the acceptance angle of a newly built pressure cell. This limit exceeds the upper cutoff of the pressure cell used in our previous studies by a factor of 4.[16−18,21] Thus, the new pressure cell extends the pore sizes (L) accessible to SANS into the subnanometer region: $L \approx 2\pi/Q_{max} \approx 9$ Å. A powder PFAC sample was outgassed overnight at 300 °C, loaded into a thin-walled aluminum container with an internal thickness of 1 mm, and subsequently mounted inside the high-pressure cell. The H_2 pressure was varied from vacuum up to ∼200 bar using a home-built pressure intensifier, and all of the measurements were conducted at room temperature (∼23 °C). The scattering patterns were corrected for detector efficiency, electronic noise, and scattering from the empty pressure cell. The two-dimensional scattering patterns were radially averaged and put on an absolute scale [cross section $I(Q)$ in cm^{-1}] by means of precalibrated secondary standards. The scattering patterns from the PFAC under vacuum and at different H_2 pressures (Figure 1) show that $I(Q)$ increases continuously with pressure for all values of the scattering vector. The observed variation of $I(Q)$ is due to the cumulative effect of the densification of the adsorbed H_2 in pores and the increasing incoherent background from H_2 with pressure.

The pressure-dependent contribution of the incoherent background (I_{inc}) was determined by fitting the experimentally measured functions $I(Q)$ at each pressure to the Debye equation:[22]

$$I(Q) = \frac{B}{(a^{-2} + Q^2)^2} + I_{inc} \quad (2)$$

where B is a pressure-dependent variable that accounts for the strong variation of the scattering-length density of H_2 with pressure and a is the Debye correlation length in the autocorrelation function of the scattering-length density fluctuations $\gamma(r) = \exp(-r/a)$; a is independent of pressure for completely saturated pores. The fits were performed over the range Q > 0.1 Å^{-1}, and the obtained values of I_{inc} (Figure 1) were subtracted from the experimentally measured intensities to provide the coherent cross sections $I_{coh}(Q)$. As explained in the SI, the density of H_2 in the pores $(\rho_{H_2})_{pore}$ at different values of Q (or, equivalently, at different pore sizes $L \approx 2\pi/Q$) can be evaluated using the ratios of the coherent intensities measured for H_2-loaded and blank carbons [$I_{coh}(Q, P)$ and $I_{coh}(Q, P = 0)$, respectively]:

$$\frac{I_{coh}(Q,P)}{I_{coh}(Q,P=0)} = [1 + 5.6(\rho_{H_2})_{pore}]^2 \quad (3)$$

dx.doi.org/10.1021/ja202432x |J. Am. Chem. Soc. 2011, 133, 13794–13797

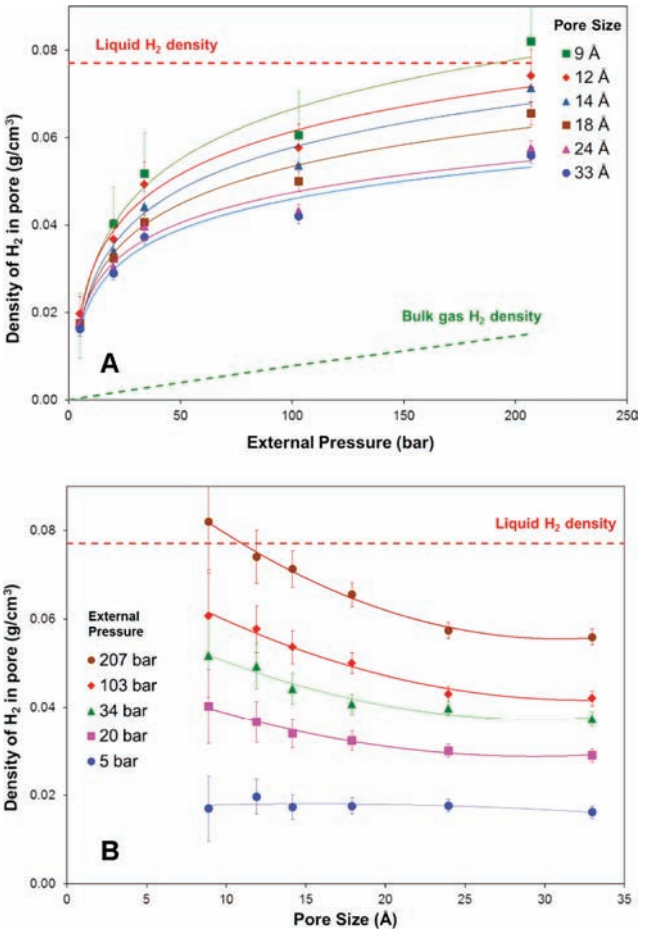

Figure 3. Room-temperature densities of adsorbed H_2 as functions of (A) pressure for selected pore sizes and (B) pore size at constant pressures.

The ratios of coherent intensities under vacuum and at various P are plotted in Figure 2 for the Q range of interest. Six Q values corresponding to maxima in the pore size distribution profile of the PFAC sample (shown in the SI) were selected for density calculations and are noted in Figure 2. The corresponding errors in the coherent intensity ratios (estimated after reduction of the raw data) are also shown. These errors were used to calculate subsequent errors in the density, the densification factor, and P_{int} using error propagation theory.

The densities of H_2 in carbon pores calculated using eq 3 are plotted in Figure 3A as functions of pressure for the selected pore sizes. The densities of liquid H_2 at the triple point and gaseous H_2 at the corresponding pressures at room temperature are also shown for comparison. It is evident that at room temperature, for any given values of P_{ext} and pore size, the density of *confined* H_2 is considerably higher than that of the bulk gas and approaches the density of liquid H_2 at the highest pressure for the narrowest pore studied. The effect of pore size on the density at constant pressure is clearly illustrated in Figure 3B: the density is systematically higher in the narrow pores and decreases with increasing pore size, reaching almost constant values in the mesoporous range (>20 Å). These results clearly demonstrate the advantage of adsorptive storage over compressed gas storage and emphasize the greater efficiency of micropores over mesopores in the adsorption process.

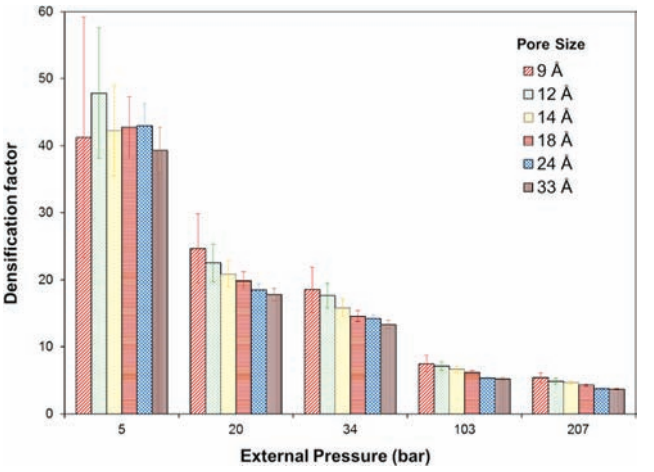

Figure 4. Room-temperature densification factors of adsorbed H_2 at different external pressures.

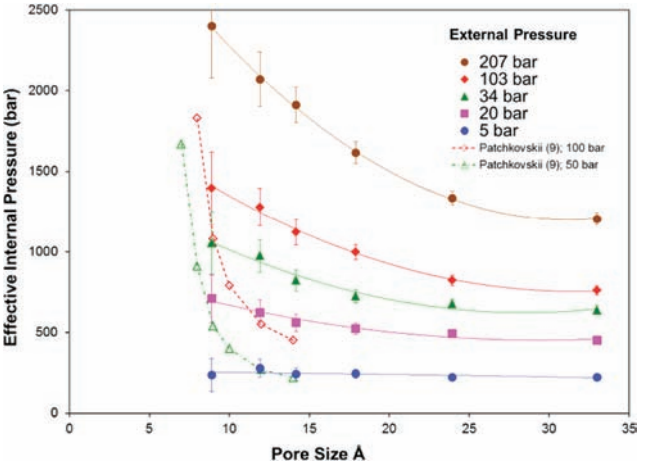

Figure 5. Internal H_2 pressures within PFAC nanopores derived from room-temperature density values of adsorbed H_2 as a function of P_{ext}. P_{int} values predicted using the model of Patchkovskii et al.[9] at 50 and 100 bar are also shown for comparison.

The densification factors (i.e., the ratio of the adsorbed and bulk gas densities) at various pressures at $T = 23$ °C are shown in Figure 4. The ratio is higher at the lowest pressures (40−50 times higher than the bulk density) and decreases with pressure. The decreasing trend of P_{int} with increasing P_{ext} is a consequence of the nonequivalence of adsorption sites: the strongest binding sites (where the local P_{int} is the highest) are occupied first (at low P_{ext}), while the weaker binding sites (with low P_{int}) contribute to adsorption only at higher P_{ext}.

As discussed earlier, the overlap of the potentials of opposite walls in nanoscale pores induces extensive densification of the confined fluid, greatly exceeding the fluid density next to an open flat surface. This effect is equivalent to developing an effective "internal" pressure in carbon pores that may exceed by orders of magnitude the external pressure applied to the system.[9−12] To quantify this effect of confinement, we calculated the effective internal pressure corresponding to each H_2 density in pores using the nonideal equation of state for H_2.[23] The results in Figure 5 demonstrate that P_{int} within the 9 Å pores varies between 240

dx.doi.org/10.1021/ja202432x |*J. Am. Chem. Soc.* 2011, 133, 13794–13797

and 2400 bar as P_{ext} increases from 5 to 207 bar. The difference between P_{int} and P_{ext} decreases with P_{ext} as well as with the pore size, in general agreement with theoretical predictions[9] (Figure 5). However, the variation of the experimentally observed P_{int} as a function of pore size is less pronounced than predicted,[9] reflecting the fact that theoretical predictions depend greatly on the strength of the adsorption interactions assumed in the calculations.

Although various theoretical models consistently predict that H_2 adsorption occurs preferentially in the nanopores of solid adsorbents,[11−13,24] providing experimental evidence for such behavior is not possible using "traditional" volumetric or gravimetric adsorption methods. The results reported here represent the first experimental characterization of the phase behavior of H_2 confined in the pores of a carbon adsorbent as a function of pore size and pressure. They provide experimental evidence that adsorptive gas storage is more efficient at low pressures than at elevated pressures and that the adsorption process occurs most effectively in small pores. To put these findings into perspective, if a carbon adsorbent containing 1 cm^3/g of pores with widths of only 9 Å could be synthesized, the amount of H_2 that could be stored at room temperature and 207 bar would be 8.13 wt %. This uptake (material-based) may approach the DOE system-based target for 2010 (4.5 wt %).[1] We hope that these findings will provide new guidance for the synthesis of porous carbons with tailored/optimized structures and initiate further theoretical considerations explaining fluid densification far away from the liquid−gas critical point.

■ ASSOCIATED CONTENT

Supporting Information. Detailed synthesis of PFAC, characterization details, and model equations for SANS. This material is available free of charge via the Internet at http://pubs.acs.org.

■ AUTHOR INFORMATION

Corresponding Author
gallegonc@ornl.gov; melnichenkoy@ornl.gov

■ ACKNOWLEDGMENT

This research was sponsored by the Materials Science and Engineering Division, Office of Basic Energy Sciences, U.S. Department of Energy. SANS experiments were conducted at ORNL's High Flux Isotope Reactor, sponsored by the Scientific User Facility Division, Office of Basic Energy Sciences, U.S. Department of Energy. D.S. and L.H. acknowledge appointments under the ORNL Postdoctoral Associate Program administered jointly by Oak Ridge Institute for Science and Education/Oak Ridge Associated Universities and ORNL. The authors acknowledge helpful discussions with Dr. J. Morris (ORNL) and assistances with PFAC synthesis by V. Bhat and with instrumentation by Dr. T. Blach.

■ REFERENCES

(1) Stetson, N. T. "Hydrogen Storage" 2010 Annual Merit Review and Peer Evaluation Meeting, U.S. DOE. http://www.hydrogen.energy.gov/pdfs/review10/st00a_stetson_2010_o_web.pdf (accessed March 7, 2011).
(2) Schlapbach, L.; Zuttel, A. *Nature* **2001**, *414*, 353.
(3) Crabtree, G. W.; Dresselhaus, M. S. *MRS Bull.* **2001**, *33*, 421.
(4) Dillon, A. C.; Heben, M. J. *Appl. Phys. A: Mater. Sci. Process.* **2001**, *72*, 133.
(5) Thomas, K. M. *Catal. Today* **2007**, *120*, 389.
(6) Benard, P.; Chahine, R. *Scr. Mater.* **2007**, *56*, 803.
(7) Tanaka, H.; Kanoh, H.; El-Merraoui, M.; Steele, A. A.; Yudasaka, M.; Ijima, S.; Kaneko, K. *J. Phys. Chem. B.* **2004**, *108*, 17457.
(8) Liu, Y.; Kabbour, H.; Brown, C. M.; Neuman, D. A.; Ahn, C. C. *Langmuir* **2008**, *24*, 4772.
(9) Patchkovskii, S.; Tse, J. S.; Yurchenko, S. N.; Zhechkov, L.; Heine, T.; Seifert, G. *Proc. Natl. Acad. Sci. U.S.A.* **2005**, *102*, 10439.
(10) Peng, L.; Morris, J. *J. Phys. Chem. C* **2010**, *114*, 15522.
(11) Cabria, I.; Lopez, J.; Alonso, J. A. *Carbon* **2007**, *45*, 2649.
(12) Aga, R. S.; Fu, C. L.; Krcmar, M.; Morris, J. R. *Phys. Rev. B* **2007**, *76*, No. 165404.
(13) Rzepka, M.; Lamp, P.; de la Casa-Lillo, M. A. *J. Phys. Chem. B* **1998**, *102*, 10894.
(14) Gogotsi, Y.; Portet, C.; Osswald, S.; Simmons, J. M.; Yildrim, T.; Laudision, G.; Fisher, J. E. *Int. J. Hydrogen Energy* **2009**, *34*, 6314.
(15) de la Casa-Lillo, M. A.; Lamari-Dakrim, F.; Cazorla-Amoros, D.; Linares-Solano, A. *J. Phys. Chem. B* **2002**, *106*, 10930.
(16) Melnichenko, Y. B.; Mayama, H.; Cheng, G.; Blach, T. *Langmuir* **2010**, *26*, 6374.
(17) Melnichenko, Y. B.; Radlinski, A. P.; Mastalerz, M.; Cheng, G.; Rupp, J. *Int. J. Coal Geol.* **2009**, *77*, 69.
(18) Melnichenko, Y. B.; Wignall, G. D. *Int. J. Thermophys.* **2009**, *30*, 1578.
(19) Burket, C. L.; Rajagopalan, R.; Marencic, A. P.; Dronvajjala, K.; Foley, H. C. *Carbon* **2006**, *44*, 2957.
(20) General-purpose SANS instrument (CG-2). http://neutrons.ornl.gov/instruments/HFIR/factsheets/Instrument_cg2.pdf (accessed Aug 6, 2011).
(21) Radlinski, A. P.; Busbridge, T. L.; Mac, E.; Gray, A.; Blach, T.; Cheng, G.; Melnichenko, Y. B.; Cookson, D. J.; Mastalerz, M.; Esterle, J. *Langmuir* **2009**, *25*, 2385.
(22) Debye, P.; Anderson, H. R.; Brumberger, H. *J. Appl. Phys.* **1957**, *28*, 679.
(23) Lemmon, E. W.; McLinden, M. O.; Friend, D. G. Thermophysical Properties of Fluid Systems. In *NIST Chemistry WebBook*; NIST Standard Reference Database; National Institute of Standards and Technology: Gaithersburg MD; http://webbook.nist.gov (accessed July 30, 2011).
(24) Jagiello, J.; Anson, A.; Martinez, M. T. *J. Phys. Chem. B* **2006**, *110*, 4530.